Al-Qadisiyah JournalFor Engineering Sciences 18 (2025) 368 – 377

Contents lists available at: http://qu.edu.iq

Al-Qadisiyah Journal for Engineering Sciences

Journal homepage: https://qjes.qu.edu.iq

Research Paper

Efficient iron removal from petroleum refinery wastewater using RCC-natural clay ceramic adsorbents: An isotherm and kinetic study

Netty Herawati [1,2], ***Subriyer Nasir*** [1] ✉, ***Kiagus A. Roni*** [2], ***and Muhammad A. Karim*** [2]

[1] *Department of Chemical Engineering, Universitas Sriwijaya, Jl. Raya Palembang–Prabumulih, Ogan Ilir 30662, Indonesia.*
[2] *Chemical Engineering Study Program, Universitas Muhammadiyah Palembang, Jl. Jenderal A. Yani 13 Ulu, Plaju, Palembang 30137, Indonesia.*

ARTICLE INFO

Article history:
Received 07 June 2025
Received in revised form 05 August 2025
Accepted 12 October 2025

keyword:
Freundlich isotherm
Langmuir
Isotherm
Natural clay
Spent Catalyst

ABSTRACT

The treatment of petroleum refinery wastewater (PRW) continues to pose a serious environmental issue, particularly due to its high content of heavy metals, especially iron (Fe). This study investigates the adsorption performance and kinetics of iron removal from synthetic petroleum refinery wastewater using ceramic adsorbents formulated from a mixture of clay and RCC spent catalysts. The adsorbent is prepared from a mixture of clay and RCC spent catalysts (ratio 1:1) and evaluated through both batch adsorption systems. Adsorption efficiency was tested at different adsorbent dosages (2.5, 5.0, and 7.5 g), contact times (5-60 minutes), and initial iron concentrations (20-100 mg/L). This study successfully demonstrated the high efficiency of ceramic-based adsorbents in removing iron ions from petroleum refinery wastewater. The maximum removal efficiency of 99.94% was achieved under batch conditions using 2.5 g of adsorbent at an initial iron concentration of 40 mg/L with a contact time of 60 minutes. Adsorption equilibrium and kinetic analyses confirmed that the process well described the Langmuir isotherm and pseudo-second order kinetic models, suggesting monolayer chemisorption on a homogeneous surface with strong interactions between iron ions and the reactive surface site on the adsorbent. The strong linear correlation coefficients ($R^2 > 0.98$ and $R^2 > 0.99$, respectively) confirmed the reliability of these models in describing the adsorption mechanism. The use of RCC spent catalyst as a low-cost, thermally stable, and sustainable adsorbent material contributes to both wastewater remediation and industrial waste valorization.

1. Introduction

The rapid expansion of the petroleum industry has raised significant environmental concerns, particularly in waste management practices. Among the various products generated during oil and gas production, petroleum refinery wastewater (PRW) is one of the abundant and environmentally challenging waste streams. Originating from subsurface reservoirs that typically contain a mixture of crude oil, oil and grease, heavy metal, and water, PRW is continuously released to the surface as part of oil and gas extraction processes [1,2]. Due to its complex composition and high volume, PRW is recognized as one of the most critical sources of industrial wastewater associated with hydrocarbon production [3, 4]. In South Sumatra, for instance, an oil and gas company operates 201 production wells and 73 injection wells, with approximately 80% of the PRW discharged directly into the surrounding environment [5]. PRW is a highly complex effluent comprising a wide range of organic and inorganic constituents. Globally, its daily generation is estimated at approximately 250 million barrels, of which exceeding 40% is released into the surrounding ecosystem without adequate treatment [6, 7]. PRW, which is known as produced water, cannot be discharged or reused directly due to the presence of several contaminants such as total dissolved solids (TDS), hydrocarbons, oil and grease, and heavy metals [8]. If improperly managed, PRW can contaminate surface water, groundwater, and soil. Treatment technologies including physical, chemical, and biological methods have been extensively studied and implemented to mitigate these impacts [9, 10]. Typically, the oil-to-PRW ratio in many wells is about 1:3 [9, 11]. Among the major pollutants, heavy metals such as iron (Fe), cadmium (Cd), lead (Pb), and mercury (Hg) pose significant environmental and health hazards [12]. Iron is commonly found in PRW, with reported concentrations ranging from 0.1 to 1100 mg/L [13]. It has the potential to cause environmental degradation and operational challenges, such as corrosion. The effective removal of iron from PRW is imperative before any reuse or discharge into the environment. Several techniques have been applied to remove iron contaminants, including chemical precipitation, membrane-based separation, and electrocoagulation. Among these, adsorption has attracted growing interest due to its cost-effectiveness, ease of operation, and high removal performance [14]. In South Sumatra, a catalytic cracking unit operated by one of the oil and gas companies produces approximately 15.98 (tons) of spent residue catalytic cracking (RCC) catalysts each year. At present, this material is stored in hazardous waste facilities without any further application [15]. Given its composition and availability, RCC shows considerable potential as a low-cost adsorbent for PRW water treatment. Although previous studies have explored the potential of ceramic materials for heavy metal removal, there is still a lack of detailed understanding regarding the adsorption kinetics of iron on these adsorbents under various conditions. In this study, the RCC catalyst was activated before use. The activation process for the spent RCC catalyst was carried out by calcining it at 900 C° for 2 (hours) [16]. This step aims to remove remaining organic compounds, improve thermal stability, and open pores in the material structure, thereby increasing the surface area and enriching active sites for adsorption. The choice of 900 C° was based on previous references showing that this temperature is effective enough to activate aluminosilicate-based materials such as RCC without causing significant sintering.

*Corresponding Author.
E-mail address: subriyer@unsri.ac.id ; Tel: (08) 127-992 9595 (Subriyer Nasir)

https://doi.org/10.30772/qjes.2025.161210.1588
2411-7773

Nomenclature

AAS	Atomic Absorption Spectrophotometer	C	The equilibrium concentration of adsorbate in solution (mg/L)
BET	Braeuer–Emmett–Teller	C_e	Iron concentration at equilibrium (mg/L)
EDX	Energy-dispersive X-ray spectroscopy	C_o	Intensity and heterogeneity of the adsorption process
EOR	Enhanced oil recovery	K_f	Freundlich constant reflecting the adsorption capacity of the adsorbent $(L/mg)^{1/n}$
$FTIR$	Fourier Transform Infrared Spectroscopy	k_1	The kinetic constant of pseudo-first-order adsorption $(1/min)$
PRW	petroleum refinery wastewater	k_2	The kinetic constant of pseudo-second-order adsorption $(g/mg.min)$
PFO	Pseudo-first-order	K_L	Langmuir constant that indicates the binding strength between adsorbent and adsorbate (L/mg)
PSO	pseudo-second-order	n	Freundlich exponent that represents the initial concentration of adsorbate (mg/g)
RCC	Residue Catalytic cracking	Q_e	Maximum adsorption capacity corresponding to monolayer coverage on the surface (mg/g)
$RMSE$	Root Mean Square Error	q_e	Adsorption capacity at equilibrium (mg/g)
SEM	scanning electron microscopy	q_t	Amount of adsorbate adsorbed at time t (mg/g)
TDS	total dissolved solids	q_{max}	The maximum adsorption capacities
R^2	Correlation coefficient	t	Duration of contact between the adsorbent and the solution (min.)
v	Volume of the solution (L)		

The calcination process was carried out in a furnace with gradual temperature control to prevent cracking or damage to the physical structure of the adsorbent. A study demonstrated that synthesized $\gamma - Al_2O_3$ effectively reduced iron levels in PRW to 0.0014 ppm, achieving a removal efficiency of 99.9% [17]. A more recent study reported that modified silica showed even higher efficiency in eliminating iron from PRW. Specifically, at a contact time of 60 minutes and pH 7, maximum removal efficiencies of 99.99% and 99.98% were achieved using modified silica doses of 0.4 mg/L and 0.2 mg/L, respectively [18]. The present research focuses on investigating the adsorption behavior of iron ions from petroleum refinery wastewater using ceramic-based adsorbents synthesized from a combination of natural clay and RCC spent catalysts. Both isotherm models and adsorption kinetics were evaluated to better understand the iron removal mechanism. The initial characterization of real produced water (PRW) collected from an oil and gas facility in South Sumatra revealed an iron concentration of 0.51 mg/L, which exceeds the maximum permissible limit of 0.3 mg/L for wastewater discharge, as stipulated by the Indonesian Ministry of Environment (*Regulation No. 5/2013*). This emphasizes the critical need for effective treatment before discharge or potential reuse.

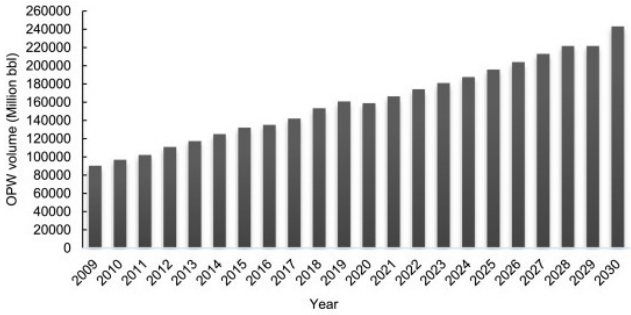

Figure 1. Recent global statistics on PRW [7].

2. Materials and methods

2.1 Preparation of ceramic adsorbents

In this study, RCC was first activated. The activation process for RCC was carried out by calcination at 900 C°for 2 (h) [16]. Activation aims to remove remaining organic compounds, improve thermal stability, and open pores in the material structure, thereby increasing the surface area and enriching active sites for adsorption. The choice of a temperature of 800-900 C°was based on previous references showing that this temperature is quite effective for activating aluminosilicate-based materials such as RCC without causing significant sintering. The calcination process was carried out in a furnace with gradual temperature control to prevent cracking or damage to the physical structure of the adsorbent. Figure 1 shows the raw materials used in this study, comprising natural clay sourced from a local brick manufacturer in Palembang and RCC waste from a petroleum refinery in South Sumatra, Indonesia. Both materials were sieved to 100 (Mesh) and mixed at a 1:1 weight ratio. Demineralized water was added to achieve a uniform consistency, and the mixture was molded into cylindrical tablets (10 mm diameter, 10 mm thickness). The specimens were sun-dried and calcined at 900 C°for 24 (h). The morphological and elemental characteristics of the ceramic adsorbents were analyzed through scanning electron microscopy coupled with energy-dispersive X-ray spectroscopy (SEM-EDX).

(a) RCC spent catalyst (b) Clay

Figure 2. Materials for ceramic adsorbent.

Figure 2 presents the initial morphology of the ceramic adsorbent, showing a heterogeneous mixture of cylindrical and rounded pellets with beige to light brown color. The relatively smooth and homogeneous surface suggests a high availability of active sites [19]. Variations in color and texture indicate the natural heterogeneity of raw materials and imply a porous structure favorable for adsorption, as supported by the uniform pellet shape and granularity. Based on the mineral composition of the ceramic adsorbent and the observed changes in elemental content after adsorption, it is plausible that ion exchange played a role in the removal of iron ions. The exchange of iron with native cations from the clay and RCC matrix is consistent with known cation exchange mechanisms in aluminosilicate-based materials. Clay contains negatively charged sites that can exchange previously adsorbed ions (such as Na^+, Ca^{2+}) with Fe^{2+} ions from solution.

2.2 Adsorption study

To study the batch adsorption of iron, analytical-grade ferrous sulfate heptahydrate ($FeSO_47H_2O$, Merck) was used without further purification. Synthetic PRW containing iron ions was prepared by dissolving $FeSO_47H_2O$ in distilled water to obtain solutions with varying initial concentrations ranging from 20 to 100 mg/L. In this study, we simulated the composition of refinery wastewater by preparing a solution containing iron derived from $FeSO_47H_2O$ to investigate the adsorbent's capacity in removing a single target ion. Batch adsorption experiments were performed to assess the performance of the ceramic-based adsorbents under different parameters. The influence of adsorbent dosage (2.5, 5.0, and 7.5 g), contact time (5, 15, 30, 45, and 60 minutes), and initial iron concentration (20–100 mg/L) on adsorption efficiency was systematically investigated. Iron concentrations were determined using an Atomic Absorption Spectrophotometer (Shimadzu AA-7000). The use of higher Fe concentrations (20–100 mg/L) in the synthetic system to the selected concentration range reflects elevated contamination levels that may occur during operational upsets or in PRW from other fields or enhanced oil recovery (EOR) sites, where Fe concentrations have been reported to be significantly higher (0.1-1100 mg/L) [13]. Higher concentrations are essential to observe clear adsorption behavior and generate meaningful data for kinetic and isotherm modeling, ensuring accurate parameter estimation and understanding of the adsorbent's capacity under stress conditions.

2.3 Adsorption and kinetic analysis

Batch adsorption experiments were conducted to evaluate the removal efficiency of iron ions using ceramic adsorbents derived from RCC waste and natural clay. All experiments were carried out at room temperature (±27 C°) under controlled conditions. A series of 250 mL Erlenmeyer flasks was filled

with 100 mL of synthetic iron solution, prepared by dissolving $FeSO_4 7H_2O$ in deionized water to obtain initial concentrations ranging from 20 to 100 mg/L. The solution pH was adjusted to pH 11 for each experiment. A specific mass of ceramic adsorbent (2.5g, 5.0g, or 7.5g) was added into each flask. The flasks were placed in a mechanical orbital shaker and agitated at 100 rpm for varying contact times (5, 15, 30, 45, and 60 minutes). After the designated time, the mixture was filtered using Whatman filter paper, and the residual iron concentration in the filtrate was determined using Atomic Absorption Spectrophotometry (AAS). The adsorption capacity of ceramic adsorbent (q_e) was calculated using the following Eq. 1, [20]:

$$q_e = (C_o - C_e) \times \frac{v}{m} \tag{1}$$

Where: q_e denotes the adsorption capacity at equilibrium (mg/g), C_o represents the initial concentration of iron in the solution (mg/L), C_e is the iron concentration at equilibrium (mg/L), v indicates the volume of the solution (L), and m refers to the mass of the adsorbent used (g). The percentage of iron removed was determined using the following formula, Eq. 2:

$$Removal(\%) = \frac{(C_{in} - C_{out})}{C_{in}} \times 100 \tag{2}$$

WhereC_{in} is the initial iron concentration (mg/L) and C_{out} is the final iron concentration (mg/L).

Table 1. Isotherm and kinetic equations.

Model	Linear Equation	Equation	Ref.
Langmuir	$\frac{C_e}{q_e} = \frac{1}{Q_e K_1} + \frac{C_e}{Q_e}$	(3)	[21,22]
Freundlich	$\log q_3 = \log K_f + \frac{1}{n} \log C_e$	(4)	[23,24]
Pseudo 1st order	$\ln(q_e - q_t) = \ln q_e - \frac{K_1}{2303} t$	(5)	[25,26]
Pseudo 2nd order	$\frac{t}{q_t} = \frac{1}{K_2 q_e^2} + \frac{1}{q_e} t$	(6)	[27,28]

3. Results and discussion

3.1 SEM and EDX analysis

Scanning electron microscopy (SEM) observations revealed significant differences in the surface morphology of the ceramic adsorbent before and after adsorption, can be seen in Fig. 3.

(a) Before adsorption (b) After adsorption

Figure 3. Ceramic adsorbents steps.

Before adsorption, the adsorbent surface appeared relatively smooth with densely packed particles and limited porosity. Figure 4 show the surface was homogeneous with few cracks or open voids, which indicated that most active sites were still unutilized or not fully exposed as seen in Fig. 4a. After adsorption, Fig. 4b, the morphology changed significantly, characterized by increased surface roughness, the appearance of fissures, and more pronounced porous structures. The surface appeared to undergo restructuring, likely due to interactions between Fe ions and the reactive sites present on the adsorbent surface. The particle agglomeration became denser, and the texture more complex, indicating intensified physical and chemical interactions during the adsorption process.

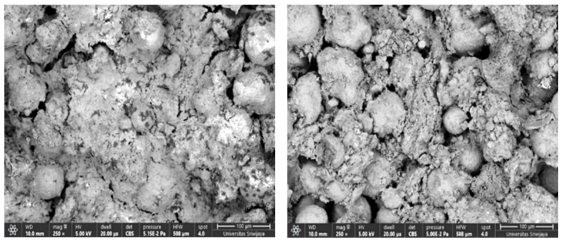

(a) Before adsorption (b) After adsorption

Figure 4. Scanning Electron microscope ceramic adsorbent (a) before adsorption (b) after adsorption.

Energy dispersive X-ray spectroscopy (EDX) analysis also indicated changes in elemental composition before and after iron adsorption. Before adsorption, dominant elements detected included carbon (C), oxygen (O), silicon (Si), aluminum (Al), titanium (Ti), and iron (Fe). After adsorption, several changes were observed, including an increase of O, Si, Al, and Fe content, as well as a reduction in the content of C and the loss of Ti element. These changes suggest an involvement of surface functional groups in interactions with Fe ions and possible modifications to the adsorbent surface structure. The variations in elemental composition and surface morphology indicate that the iron ion adsorption process involves not only surface-level interactions but also triggers both textural and chemical modifications to the adsorbent.

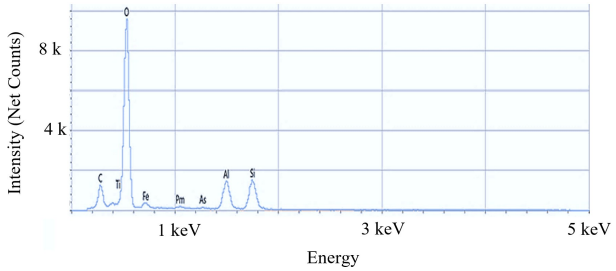

(a) Before adsorption

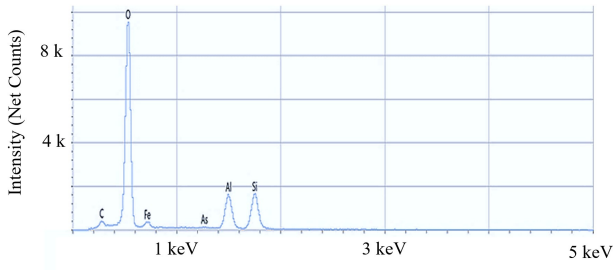

(b) After adsorption

Figure 5. Spectrum EDX ceramic adsorbent (a) before adsorption (b) after adsorption.

Figure 5a shows that the main elements detected are oxygen, indicating the presence of metal oxides or silicates, the main component of clay and RCC. Carbon can come from residual organic materials or the synthesis process. Silicon and aluminum indicate basic materials such as kaolin or aluminosilicates, which are common in ceramics and RCC, while iron may come from the initial composition of RCC or minor contaminants. Figure 5b shows that the EDX spectrum after the adsorption process using ceramic adsorbents shows several elements that are still detected: O, C, Si, Al, and Fe are still dominant, indicating that the ceramic structure has not changed significantly. This indicates the possibility of interaction with the adsorbent surface.

Table 2. EDX elemental composition before and after adsorption.

Element	C	O	Al	Si	Ti	Fe	As	Pm
Wt.% (before)	03.50	37.20	11.90	16.20	12.20	06.70	00.50	11.80
Wt.% (after)	01.60	46.40	18.00	25.10	—	08.40	00.50	—

Table 2 presents a comparative analysis of the elemental composition of the ceramic adsorbents before and after the adsorption process, as determined by EDX spectroscopy. Table 2 displays a comparative analysis of the elemental composition on the surface of the ceramic adsorbent before and after iron ion adsorption, expressed in weight percent (wt.%). The observed variations in several elemental concentrations highlight the presence of both physical and chemical interactions between iron ions and the functional groups present on the adsorbent surface. Notably, the carbon content decreased from 3.5% to 1.6% following adsorption, which is likely attributed to the removal or desorption of weakly bound organic carbon compounds during stirring and rinsing procedures. Such a reduction is particularly plausible under aqueous conditions, where loosely attached or soluble organic matter can be easily eliminated from the surface. This decline in carbon levels implies that the adsorption process is primarily governed by inorganic surface functionalities, potentially involving silicate, aluminate, or metal oxide groups, rather than organic moieties. Moreover, elemental profiling before and after adsorption revealed marked alterations in the levels of aluminum (Al) and silicon (Si), indicating their active participation in the adsorption mechanism. The disappearance of the titanium peak in the post-adsorption EDX spectrum suggests that Ti on the adsorbent surface was either masked by newly adsorbed Fe species, diluted due to surface compositional changes, or displaced during the batch contact process. This observation highlights the dynamic nature of surface chemistry in ceramic adsorbents derived from RCC catalysts. The increase in iron from 6.7% to 8.4% confirmed that Fe^{2+} adsorption on the adsorbent surface was successful. This is in line with the expected performance of high-affinity ceramic adsorbents, such as aluminosilicates or RCC components. Overall, the observed increase in element concentrations supports the conclusion that surface complexation and ion exchange mechanisms play a dominant role in the capture of iron ions, further demonstrating the high affinity and surface reactivity of the adsorbent toward heavy metals.

3.2 Fourier Transform Infrared Spectroscopy (FTIR)

The FTIR spectrum of ceramic-based adsorbent before and after iron adsorption is presented in Fig. 6.

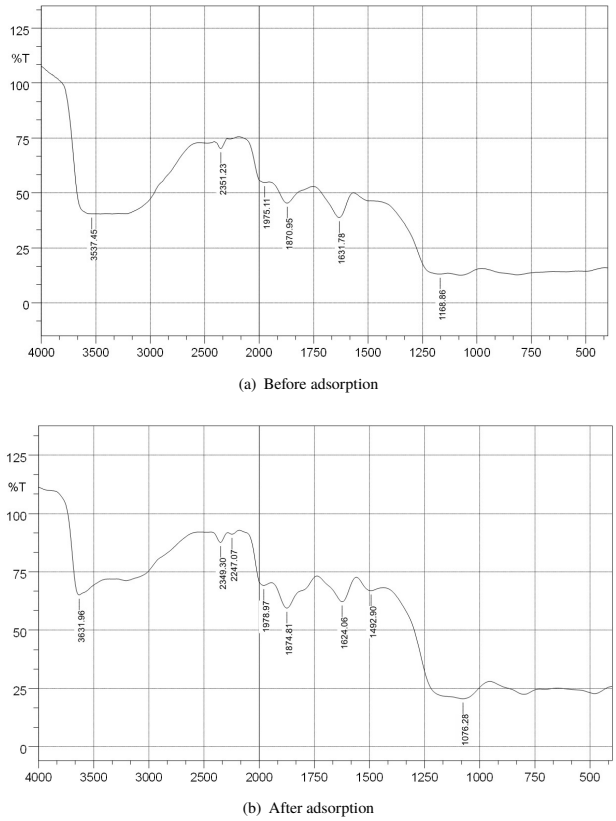

(a) Before adsorption

(b) After adsorption

Figure 6. FTIR ceramic adsorbent (a) before adsorption (b) after adsorption)

The FTIR spectra of the ceramic adsorbents before and after adsorption are shown in Fig. 6. Before adsorption, prominent absorption bands were observed at 1040 cm^{-1} and 794 cm^{-1}, corresponding to *Si–O–Si* asymmetric and symmetric stretching vibrations, typical of aluminosilicates. A broad band around 3450 cm^{-1} is attributed to –OH stretching of surface hydroxyl groups and adsorbed water, while the band at 1630 cm^{-1} represents bending vibration of H–O–H from physically adsorbed moisture. Following iron adsorption, notable shifts in peak positions and intensity were recorded. The –OH stretching band diminished in intensity, indicating the involvement of hydroxyl groups in bonding with Fe^{2+}. Additionally, the *Si–O* bands shifted slightly to lower wavenumbers, suggesting structural distortion or formation of inner-sphere complexes between Fe^{2+} and surface silanol groups. These observations are consistent with chemisorption pathways involving ligand exchange and complexation [3]. The appearance of a weak band near 580 cm^{-1} may also indicate *Fe–O* bond formation, reinforcing the hypothesis of chemical bonding rather than mere physical adherence.

3.3 Brunauer–Emmett–Teller (BET)

The specific surface area, pore volume, and pore size distribution of the ceramic-based adsorbent were determined using the Brunauer–Emmett–Teller (BET) method. The BET analysis was conducted to evaluate the surface characteristics of the ceramic-based adsorbent before and after iron adsorption. Table 3 summarizes the specific surface area, average pore diameter, and total pore volume as obtained from nitrogen adsorption–desorption isotherms. Before adsorption, the ceramic adsorbent exhibited a high specific surface area of 62.947(m^2/g), indicating a highly porous structure with abundant active sites available for interaction with iron ions. The average pore diameter was approximately 1.693 *nm* and the total pore volume was 0.134 (cm^3/g), confirming the presence of well-developed porosity conducive to effective adsorption. After the adsorption process, all parameters decreased drastically. The surface area dropped to 13.263 (m^2/g), the pore volume reduced to 0.032 (cm^3/g), and the average pore diameter slightly decreased to 19.3 *nm*. This significant reduction indicates that iron ions successfully occupied the internal pore spaces and surface-active sites of the adsorbent. These changes confirm the efficiency of the ceramic adsorbent in capturing Iron ions from solution and suggest that the adsorption process involves both surface binding and pore-filling mechanisms.

Table 3. BET Adsorbent Ceramic, before and after adsorption.

Characterization	Before	After
Specific surface area (m^2/g)	62.947	13.263
Pore size (*nm*)	1.693	19.316
Pore volume (cm^3/g)	0.134	0.032

3.4 Iron removal by ceramic adsorbents

The adsorption processes are generally classified into physical (physisorption) and chemical (chemisorption). An effective adsorbent should exhibit high affinity and surface area to ensure efficient and cost-effective removal of contaminants [29, 30]. Figure 7 presents the removal of iron at varying adsorbent dosages. A high removal (99.57%) was achieved using 2.5 *g* of ceramic adsorbent at 60 minutes and 100 mg/L initial concentration. Increasing the adsorbent dosage did not always correlate with higher efficiency, possibly due to aggregation of particles or saturation of available active sites at higher dosages. These results align closely with those reported by [17, 18], who successfully removed over 99% of the iron in their studies. The heatmaps presented in Fig. 7 show the interactive effects of duration and initial iron concentration on the adsorption efficiency using varying adsorbent masses of 2.5 *g*, 5 *g*, and 7.5 *g*. Overall, the color gradients and annotated values demonstrate a consistent trend of increasing iron removal efficiency with longer contact time and greater adsorbent dosage, while the response to initial concentration is more nuanced. At low contact times (5–15 min), the efficiency was relatively low across all concentrations, indicating limited surface interaction time. However, a significant increase was observed after 30 min, with maximum efficiency (100%) achieved at 60 min for concentrations of 60–100 (mg/L).

3.4.1 Effect of contact time

At the maximum contact time of 60 minutes, iron adsorption efficiency reached nearly complete removal across all concentrations and adsorbent dosages. For 2.5 *g*, the efficiency ranged from 98% at 20 (mg/L) to 100% at 80–100 (mg/L). Similarly, 5.0 *g* and 7.5 *g* dosages achieved 98–100% efficiency across all concentrations, indicating that 60 minutes is sufficient to reach adsorption equilibrium, regardless of initial concentration or adsorbent dose. This finding supports previous studies reporting that prolonged contact time improves active site saturation and overall adsorption capacity [27, 31].

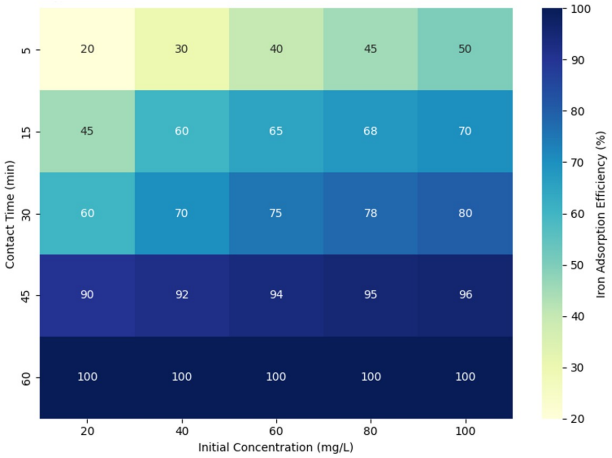

(a) Heatmap of Iron adsorption efficiency at 2.5 g Ceramic adsorbent.

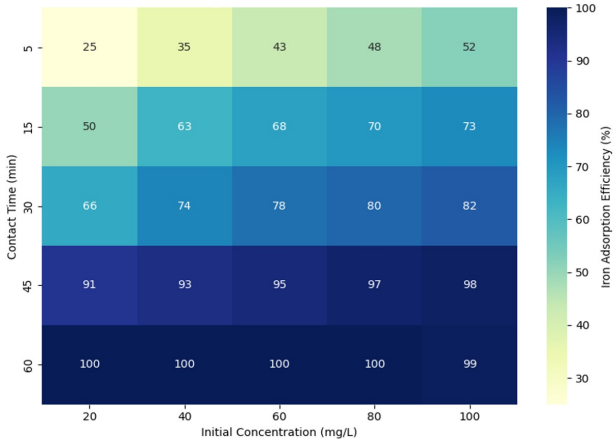

(b) Heatmap of Iron adsorption efficiency at 5.0 g Ceramic adsorbent.

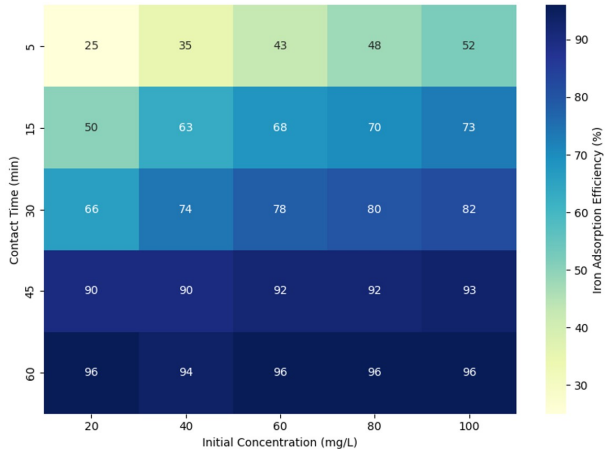

(c) Heatmap of Iron adsorption efficiency at 7.5 g Ceramic adsorbent.

Figure 7. Heatmap of iron adsorption using Ceramic adsorbent dosages at three levels.

3.4.2 Effect of initial iron concentration

The influence of initial iron concentration on adsorption efficiency was analyzed at three different adsorbent dosages: 2.5 g, 5 g, and 7.5 g, respectively. The experimental results indicate a strong interdependence between adsorbate concentration and adsorbent capacity, which varies significantly with adsorbent mass. This section discusses the observed trends and underlying mechanisms for each dosage. At the lowest adsorbent dose of 2.5 g, the system exhibited limited adsorption capacity, particularly at higher initial iron concentrations. While removal efficiency at 20 (mg/L) reached 98% within 60 minutes, a significant decline in efficiency was observed as the concentration increased. At 100 (mg/L), the adsorption efficiency plateaued at only 70%, even after 60 minutes of contact time. This decline is attributed to the rapid saturation of available active sites, which are insufficient to accommodate the elevated ion load. Furthermore, the lower adsorbent surface area-to-contaminant ratio limits the diffusion and binding of Fe^{2+} ions, resulting in reduced removal efficiency under higher loading conditions [32]. With an increased adsorbent dosage of 5 g, adsorption performance improved considerably across all concentration ranges. At 20–60 (mg/L), efficiencies of 98–100% were achieved within 45 minutes, while at 80 (mg/L), similar results were attained by 60 minutes. Even at the highest concentration of 100 (mg/L), the system reached 100% removal, demonstrating that doubling the adsorbent mass effectively mitigates site saturation and maintains sufficient surface availability. The improved performance reflects not only the greater number of active binding sites but also the enhanced dispersion and accessibility of ions across the adsorbent surface. At the highest dosage of 7.5 g, adsorption efficiency reached 100% across all initial concentrations and time intervals tested, with near-complete removal observed as early as 30–45 minutes.

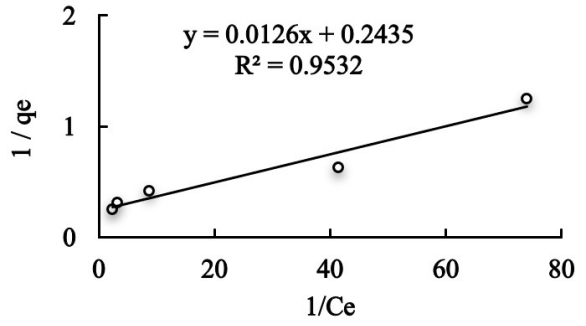

(a) Adsorbent dosages of 2.5 g.

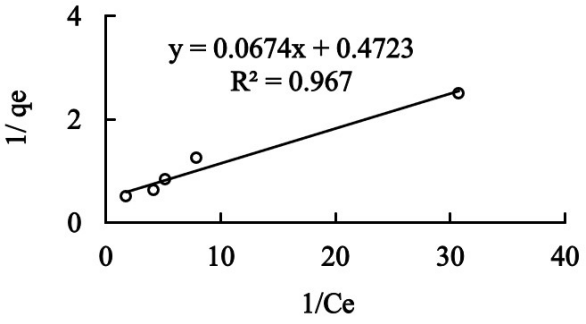

(b) Adsorbent dosages of 5.0 g.

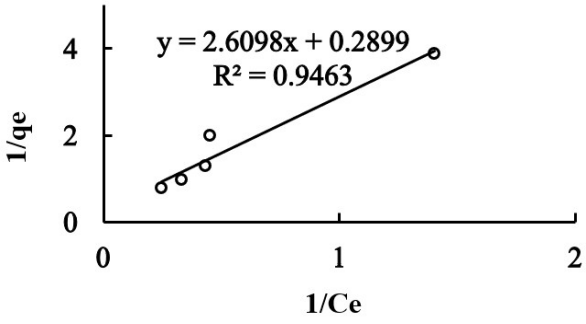

(c) Adsorbent dosages of 7.5 g.

Figure 8. Langmuir isotherm equilibrium adsorption of iron ions with various adsorbent dosages: (a) 2.5 g. (b) 5 g. and (c) 7.5 g.

This superior performance highlights the pivotal role of adsorbent dose in overcoming limitations associated with high adsorbate concentrations. The increased mass provides an excess of active sites and promotes faster diffusion

Table 4. Calculation of adsorption capacity (q_e) .

Time (min.)	Dosage (g)	Volume (L)	C_o	C_e	q_e	$1/C_e$	$1/q_e$	Iron Adsorption efficiency (%)
60	2.5	0.1	20	0.01	0.80	74.07	1.25	99.93
			40	0.02	1.60	41.49	0.63	99.94
			60	0.11	2.40	8.73	0.42	99.81
			80	0.31	3.19	3.26	0.31	99.62
			100	0.43	3.98	2.33	0.25	99.57
60	5	0.1	20	0.03	0.40	30.77	2.50	99.84
			40	0.13	0.80	7.92	1.25	99.68
			60	0.19	1.20	5.21	0.84	99.68
			80	0.24	1.60	4.14	0.63	99.70
			100	0.56	1.99	1.80	0.50	99.44
60	7.5	0.1	20	0.71	0.26	1.40	3.89	96.43
			40	2.21	0.50	0.45	1.98	94.46
			60	2.31	0.77	0.43	1.30	96.14
			80	3.01	1.03	0.33	0.97	96.24
			100	4.03	1.28	0.25	0.78	95.97

kinetics due to greater particle-particle spacing and reduced agglomeration [33]. The data indicate that, under high contaminant load conditions, sufficient adsorbent mass ensures not only enhanced removal but also shorter equilibrium times, which is critical for practical applications such as batch or continuous treatment systems.

3.4.3 Langmuir isotherm

The adsorption process conformed well to the Langmuir isotherm model, indicating monolayer adsorption onto a homogeneous surface (Langmuir model, Fig. 8). High correlation coefficients (R^2>0.94) confirmed the model's suitability for this system. The maximum adsorption capacities (q_{max}) were determined as 4.107 mg/g (2.5 g), 2.117 mg/g (5.0 g), and 3.449 mg/g (7.5 g), respectively.

3.4.4 Adsorption isotherm analysis

To further assess the applicability of the Langmuir isotherm model in describing $^{+}iron$ adsorption onto ceramic-based adsorbents, a linear plot of $\ln q_e$ versus $\ln C_e$ was constructed, as illustrated in Fig. 8. The data points used for the plot were collected at adsorption equilibrium (60 minutes) for three adsorbent dosages: 2.5 g, 5.0 g, and 7.5 g. The resulting linear regression lines indicate a strong fit with the Langmuir model, reinforcing the hypothesis that Fe^{2+} ions are adsorbed in a single-layer formation on a uniform adsorbent surface. The observed linearity also implies that the adsorption sites possess uniform energy levels and that interactions between adsorbed ions are minimal. The equilibrium adsorption capacity (q_e) values were determined using Eq. 1, with the corresponding results summarized in Table 4. Furthermore, Fig. 8 shows the plot of $\ln q_e$ versus $\ln C_e$ based on experimental data at a contact time of 60 minutes using 2.5 g of ceramic adsorbent for Fe^{2+} removal, displays a linear trend consistent with the Langmuir isotherm model. This linearity enables the determination of the Langmuir model constants as presented in Table 5. The Langmuir adsorption isotherm for Fe^{2+} ion removal yields a linear relationship is illustrates in Table 5. Suggesting that the linearized model aligns well with the experimental data. The Langmuir constants derived from the regression analysis are summarized in Table 4. The highest achievable adsorption capacities (q_{max}) were found to be 4.107 mg/g for 2.5 g adsorbent. 2.117 mg/g for 5.0 g. and 3.449 mg/g for 7.5 g. The Langmuir affinity constants (b) followed a decreasing trend with increasing adsorbent mass. With values of 19.33 (L/mg). 7.01 (L/mg). and 0.11 (L/mg), respectively. This pattern may be attributed to changes in surface accessibility and diffusion resistance at higher dosages, which can reduce the effective adsorption strength per unit mass. Furthermore, the correlation coefficients (R^2) for the linear regression equations ranged from 0.9463 to 0.9670, indicating an excellent fit between the experimental data and the Langmuir model. This strong correlation reinforces the validity of the model and confirms that monolayer adsorption is the dominant mechanism in Fe^{2+} uptake by ceramic-based adsorbents under the tested conditions.

Table 5. Langmuir isotherm constants for adsorption.

Adsorbent dosage (g)	Linear Equation	q_{max}	b	R^2
2.5	$y = 0.0126x + 0.2435$	4.107	19.33	0.9532
5.0	$y = 0.0674x + 0.4723$	2.117	7.01	0.9670
7.5	$y = 2.6098x + 0.2899$	3.449	0.11	0.9463

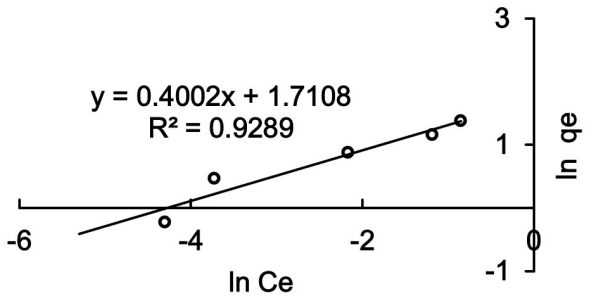

(a) Ceramic adsorbent dosage of 2.5 g.

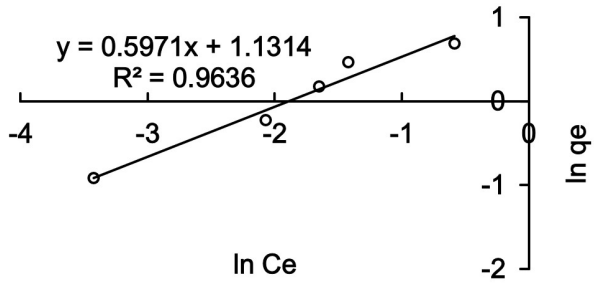

(b) Ceramic adsorbent dosage of 5 g.

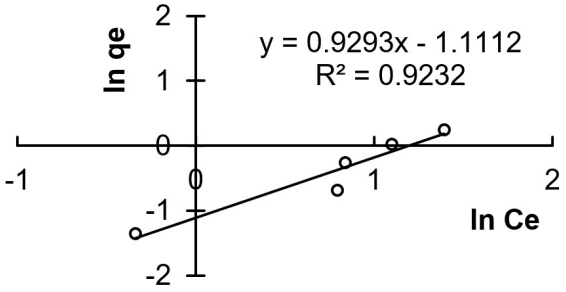

(c) Ceramic adsorbent dosage of 7.5 g.

Figure 9. Freundlich isotherm equilibrium adsorption of iron with varying ceramic adsorbent dosage (a) 2.5 g, (b) 5 g, and (c) 7.5 g.

3.4.5 Freundlich isotherm

To complement the Langmuir model, the equilibrium data were also evaluated using the Freundlich isotherm, which assumes a heterogeneous adsorption surface and multilayer adsorption behavior. This model is particularly suitable for systems where adsorption occurs on surfaces with a non-uniform distribution of energy and affinity. The linear form of the Freundlich Eq. 4, expressed as $\ln q_e$ versus $\ln C_e$, was applied to estimate the isotherm constants K_f (adsorption capacity) and $(1/n)$ (adsorption intensity). The Freundlich

isotherm exhibited R^2 values between 0.92 and 0.96, indicating a moderate correlation as shown in Fig. 9. However, the lower goodness-of-fit compared to other isotherm models implies that the adsorption process may not be fully governed by multilayer adsorption on heterogeneous surfaces. Table 6 presents the Freundlich isotherm constants derived from Fe^{2+} adsorption data. The experimental data with both Langmuir and the Freundlich models suggest that the iron adsorption mechanism involves monolayer accumulation on heterogeneous surfaces.

Table 6. Langmuir isotherm constants for adsorption.

Adsorbent dosage (g)	Linear Equation	K_f	$1/n$	R^2
2.5	$y = 0.4002x + 1.7108$	2.513	1.7108	0.9289
5.0	$y = 0.5971x + 1.1314$	3.961	1.1314	0.9636
7.5	$y = 0.9293x - 1.1112$	8.498	-1.1112	0.9232

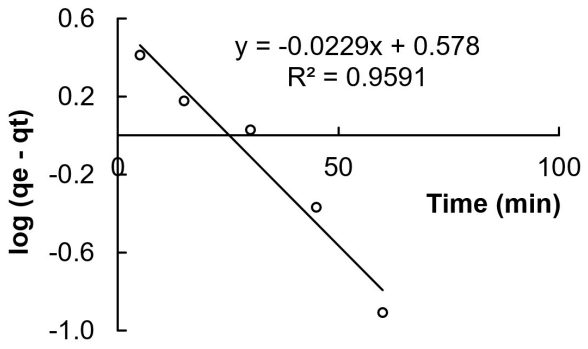

(a) Kinetics for iron ion of 2.5 g.

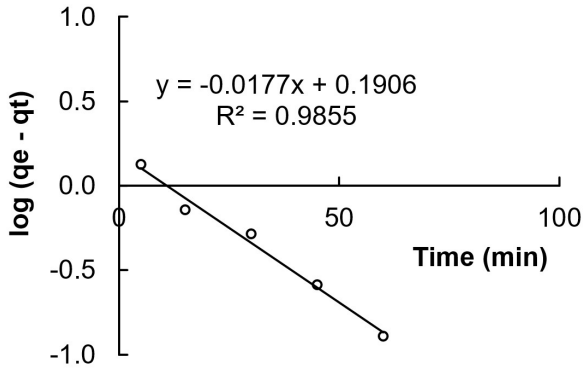

(b) Kinetics for iron ion of 5.0 g.

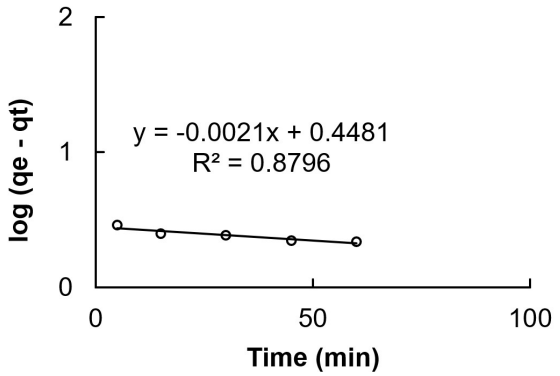

(c) Kinetics for iron ion of 7.5 g.

Figure 10. PFO adsorption kinetics for iron ion (a) 2.5 g, (b) 5 g, and (c) 7.5 g.

3.4.6 Pseudo-first-order and pseudo-second-order kinetic models

The mechanism of Fe^{2+} sorption by ceramic adsorbents is applied through two different kinetic approaches, specifically, the PFO and PSO models according to Eqs. 5 and 6. The adsorption process at a concentration of 100 (mg/L) and the mass of ceramic adsorbent are varied by 2.5 g. 5.0 g. and 7.5 g with contact times of 5 min. 15 min. 30 min. 45 min, and 60 min.

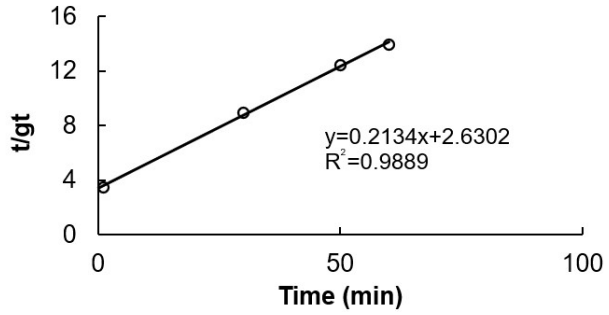

(a) Kinetics for iron ion of 2.5 g.

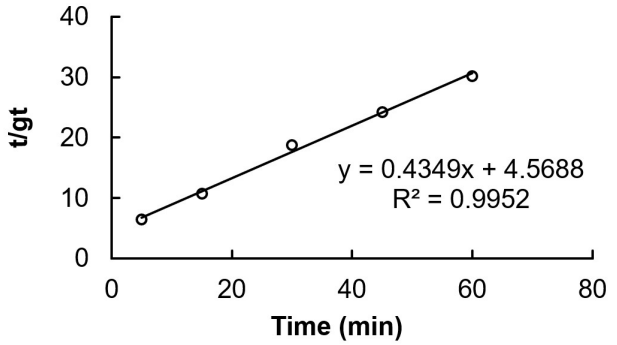

(b) Kinetics for iron ion of 5.0 g.

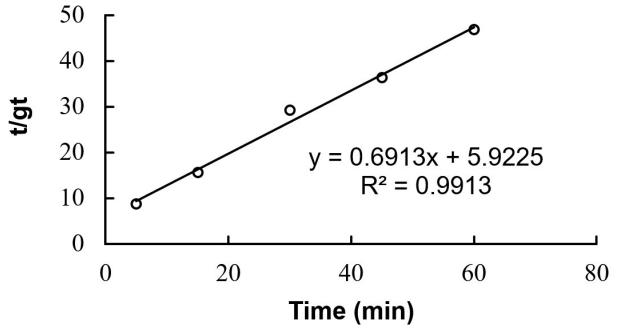

(c) Kinetics for iron ion of 7.5 g.

Figure 11. PSO adsorption kinetics for iron ion (a) 2.5 g, (b) 5 g, and c) 7.5 g.

Table 7. Parameter of kinetic model for Fe^{2+} adsorption and coefficient of determination (R^2)

Adsorbent	PFO kinetics model					
dosage (g)	Line equation	RMSE	SE	q_e	R_2	k_1
2.5	$y = 0.0229x + 0.578$	2.09	2.71	1.05	0.96	-1.331
5.0	$y = 0.020x + 0.2993$	0.64	0.83	1.04	0.96	-0.689
7.5	$y = 0.0021x + 0.4481$	0.25	0.33	1.00	0.88	-1.032
Adsorbent	**PSO kinetics model**					
dosage (g)	Line equation	RMSE	SE	q_e	R_2	k_1
2.5	$y = 0.2134x + 2.6302$	2.726	3.519	0.380	0.989	32.418
5.0	$y = 0.4349x + 4.5688$	1.374	1.774	0.219	0.995	47.997
7.5	$y = 0.6913x + 5.9225$	0.884	1.141	0.230	0.991	51.214

The data obtained was carried out with a log plot against the PFO kinetic equation, and a plot against the PSO kinetic equation can be seen in Fig. 10 and Fig. 11. The equilibrium adsorption capacity of ceramic adsorbents increases with increasing contact time. Figure 10 shows that with increasing contact time, the boundary layer resistance decreases and the mobility of metal ions in the PRW increases. Figure 11 shows that the adsorption equilibrium

Table 8. Comparison of ceramic adsorbents with various other adsorbents in terms of efficiency, cost, and environmental footprint.

	Ceramic (RCC + clay) [15, 34]	Activated carbon [35, 36]	Natural zeolite [37–39]
Fe^{2+} Adsorption Capacity	18–45 mg/g	8–30 mg/g	10–35 mg/g
Iron Removal Efficiency (%)	Up to 99.94%	80–95%	75–92%
Advantages	Resistant to extreme temperature and pH, stable	High surface area, widely available	Selective toward metal cations, low cost
Disadvantages	Limited commercial application	Non-selective to metals, prone to fouling	Lower capacity than synthetic adsorbents
Production Cost	Low	Medium–high	Low–medium
Raw Materials	RCC waste, local clay	Coconut shell, coal	Natural or synthetic
Production Emission	Low	High	Medium
Reusability	Reusable, inert	Difficult to regenerate	Regenerable
Environmental Impact	Environmentally friendly, utilizes waste	Potential waste if not regenerated	Minimal impact, easy to regenerate

increases with time. This shows that the pores of ceramic adsorbents are active enough to adsorb Fe^{2+} ions. The decrease occurred in the mass of 7.5 g_r. The corresponding linear equations for the Fe^{2+} ion adsorption kinetics and their respective R^2 values are also detailed in Table 7. Table 7 presents the adsorption kinetics of Fe^{2+} ions, which are best described by the PSO model, as indicated by correlation coefficient (R^2) values approaching unity, specifically, 0.989 for 2.5 g, 0.995 for 5.0 g, and 0.991 for 7.5 g of adsorbent. An increase in adsorbent dosage was associated with a rise in the rate constant (k), while the calculated equilibrium adsorption capacity (q_e) showed a decreasing trend. These results suggest that the contact time between the adsorbent and the solution strongly governs the rate of adsorption, consistent with a chemisorption mechanism. Furthermore, Table 7 summarizes the kinetic parameters along with the root mean square error (RMSE) and standard error (SE) for both PFO and PSO models. While the PSO model exhibited superior correlation at all adsorbent dosages, it is noteworthy that at 2.5 g the PFO model provided a lower prediction error (RMSE = 2.09, SE = 2.71), indicating a marginally better empirical fit. However, at higher adsorbent dosages (5.0 and 7.5 g), the PSO model outperformed the PFO model in both statistical correlation and predictive accuracy, thereby confirming that chemisorption becomes the dominant mechanism as the availability of active adsorption sites increases. The results confirm that the pseudo-second-order model is more accurate in explaining the adsorption kinetics of iron$^+$ ions in ceramic adsorbents, mainly due to their higher correlation and theoretical suitability with the mechanism of chemosorption. Nevertheless, error-based metrics such as RMSE and SE still provide important insights into evaluating model performance. Therefore, the selection of kinetic models should consider the balance between correlation strength and prediction accuracy, especially in practical applications involving variations in adsorbent doses. Table 8 shows a comparison of ceramic adsorbents with various other adsorbents in terms of efficiency, cost, and environmental footprint. Clay-RCC-based adsorbents have shown very promising performance in removing Fe^{2+} ions from wastewater, with efficiencies reaching 99.9%. The main advantages of this adsorbent lie in its very low cost (around 0.2–0.5 (USD/kg)) and minimal carbon footprint, as it utilizes industrial waste as the primary raw material. Furthermore, the adsorbent manufacturing process does not require high energy, making it an environmentally friendly and sustainable solution. Therefore, Clay-RCC adsorbents are ideal for large-scale applications in resource-limited regions, particularly in developing countries. Activated carbon is also a widely used adsorbent in wastewater treatment. The Fe^{2+} adsorption efficiency of activated carbon is in the range of 80–95%, slightly below the performance of other adsorbents. Its cost is moderate (1–2 (USD/kg)) and depends heavily on the source of the raw material. If produced from local biomass such as coconut shells, the carbon footprint can be significantly reduced. However, if derived from fossil fuels, the environmental impact tends to be greater. Activated carbon is a good choice for treatment systems that require flexibility and an ecological approach. Finally, natural zeolite is an adsorbent with an Fe^{2+} adsorption efficiency of between 75–92%. Its main advantages are its low cost ($<$0.5 (USD/kg)) and its low carbon footprint, as it is naturally available and does not require complex synthesis processes. Although its efficiency is lower than other adsorbents, natural zeolite is suitable for use as an initial step in water treatment systems or as a pretreatment before further adsorption. Overall, Clay-RCC offers the best balance between efficiency, cost, and sustainability, making it a superior alternative for industrial wastewater treatment applications. Activated carbon and natural zeolite are suitable for more general applications with limited costs. Considering these factors, Clay-RCC can be a strategic and sustainable solution for the management of heavy metals from wastewater.

4. Conclusions

This study successfully demonstrated the high efficiency of ceramic-based adsorbents synthesized from clay and RCC spent catalyst in removing iron ions from PRW. The highest removal rate, reaching 99.94%, was obtained under batch experimental conditions with 2.5 g of adsorbent, an initial iron concentration of 40 mg/L, and a contact time of 60 minutes. Adsorption equilibrium and kinetic analyses indicated that the process is consistent with the Langmuir isotherm and pseudo-second-order kinetic models, suggesting monolayer chemisorption on a homogeneous surface with strong interactions between iron ions and the functional groups on the adsorbent. The high correlation coefficients ($R_2 > 0.98$ and $R_2 > 0.99$, respectively) confirmed the reliability of these models in describing the adsorption mechanism. The use of RCC spent catalyst as a low-cost adsorbent material contributes to both wastewater and industrial water remediation. Future research should explore the regeneration and reuse potential of the adsorbents, as well as their performance in dynamic flow systems and real-field applications involving multi-metal or organic–inorganic pollutant mixtures. The scalability of the process can also be assessed through pilot-scale continuous column studies.

Authors' contribution

All authors contributed equally to the preparation of this article.

Declaration of competing interest

The authors declare no conflicts of interest.

Funding source

This study didn't receive any specific funds.

Data availability

The data that support the findings of this study are available from the corresponding author upon reasonable request.

REFERENCES

[1] J. Beyer, A. Goksøyr, D. Øystein Hjermann, and J. Klungsøyr, "Environmental effects of offshore produced water discharges: A review focused on the norwegian continental shelf," *Marine Environmental Research*, vol. 162, p. 105155, 2020. [Online]. Available: https://doi.org/10.1016/j.marenvres.2020.105155

[2] K. T. Amakiri, A. R. Canon, M. Molinari, and A. Angelis-Dimakis, "Review of oilfield produced water treatment technologies," *Chemosphere*, vol. 298, p. 134064, 2022. [Online]. Available: https://doi.org/10.1016/j.chemosphere.2022.134064

[3] A. Zhang, M. Li, P. Lv, X. Zhu, L. Zhao, and X. Zhang, "Disposal and reuse of drilling solid waste from a massive gas field," *Procedia Environ. Sci.*, vol. 31, no. 2, p. 577–581, 2016. [Online]. Available: https://doi.org/10.1016/j.proenv.2016.02.089

[4] E. H. Khader, T. J. Mohammed, N. Mirghaffari, A. D. Salman, T. Juzsakova, and T. A. Abdullah, "Removal of organic pollutants from produced water by batch adsorption treatment," *Clean Technol. Environ. Policy*, vol. 24, no. 2, p. 713–720, 2022. [Online]. Available: https://doi.org/10.1007/s10098-021-02159-z

[5] P. Anugrah, M. Said, and D. Bahrin, "Produced water treatment using electrocoagulation combination method with aluminum(al) and iron (fe) electrodes and activated carbon adsorption treatment," *Int. J. Adv. Sci.*

Eng. Inf. Technol., vol. 12, no. 2, p. 703–711, 2022. [Online]. Available: https://doi.org/10.18517/ijaseit.12.2.12884

[6] F. Salem and T. Thiemann, "Produced water from oil and gas exploration—problems, solutions and opportunities," *J. Water Resour. Prot.*, vol. 14, no. 2, pp. 142–185, 2022. [Online]. Available: https://doi.org/10.4236/jwarp.2022.142009

[7] K. T. Amakiri, N. A. Ogolo, A. Angelis-Dimakis, and O. Albert, "Physicochemical assessment and treatment of produced water: A case study in niger delta nigeria," *Petroleum Research*, vol. 8, no. 1, pp. 87–95, 2023. [Online]. Available: https://doi.org/10.1016/j.ptlrs.2022.05.003

[8] A. A. Novira, S. Nasir, and F. Hadiah, "Produced water treatment using the residue catalytic cracking (rcc) spent catalyst as ceramic filter material integrated with reverse osmosis (ro) system," *J. Appl. Sci. Eng.*, vol. 26, no. 3, p. 403–411, 2022. [Online]. Available: https://doi.org/10.6180/jase.202303_26(3).0011

[9] S. Jiménez, M. Micó, M. Arnaldos, F. Medina, and E. Contreras, "State of the art of produced water treatment," *Chemosphere*, vol. 192, no. 1, p. 186–208, 2018. [Online]. Available: https://doi.org/10.1016/j.chemosphere.2017.10.139

[10] K. T. Amakiri, A. R. Canon, M. Molinari, and A. Angelis-Dimakis, "Review of oilfield produced water treatment technologies," *Chemosphere*, vol. 298, no. 2, p. 134064, 2022. [Online]. Available: https://doi.org/10.1016/j.chemosphere.2022.134064

[11] S. Munirasu, M. A. Haija, and F. Banat, "Use of membrane technology for oil field and refinery produced water treatment - a review," *Process Saf. Environ. Prot.*, vol. 100, no. 1, p. 183–202, 2016. [Online]. Available: https://doi.org/10.1016/j.psep.2016.01.010

[12] A. M. Muliwa, O. A. Oyewo, and A. Maity, "Recent progress on the removal of aqueous mercury by carbon-based adsorbents: A review," *Inorg. Chem. Commun*, vol. 156, p. 111207, 2023. [Online]. Available: https://doi.org/10.1016/j.inoche.2023.111207

[13] M. A. Al-Ghouti, M. A. Al-Kaabi, M. Y. Ashfaq, and D. A. Da'na, "Produced water characteristics, treatment and reuse: A review," *J. Water Process Eng* ., vol. 28, no. 1, p. 222–239, 2019. [Online]. Available: https://doi.org/10.1016/j.jwpe.2019.02.001

[14] L. T. Hendges, T. C. Costa, B. Temochko, S. Y. Gómez González, L. P. Mazur, B. A. Marinho, A. da Silva, S. E. Weschenfelder, A. A. U. de Souza, and S. M. G. U. de Souza, "Adsorption and desorption of water-soluble naphthenic acid in simulated offshore oilfield produced water," *Process Safety and Environmental Protection*, vol. 145, pp. 262–272, 2021. [Online]. Available: https://doi.org/10.1016/j.psep.2020.08.018

[15] R. E. D. Putri, S. Nasir, and F. Hadiah, "Application of ceramic filter and reverse osmosis membrane for produced water treatment," *Pollution*, vol. 8, no. 4, p. 1103–1115, 2022. [Online]. Available: http://doi.org/10.22059/POLL.2022.337380.1343

[16] D. Anggoro, L. Buchori, and M. F. Putra, "Regeneration method for spent fcc catalysts: Brief review," *J. Res. Chem.*, vol. 4, no. 2, p. 49–53, 2023. [Online]. Available: https://doi.org/10.22271/reschem.2023.v4.i2a.96

[17] Z. Karm, A. D. Subhi, and R. S. Hamied, "Synthesis, characterization and application of gamma-alumina as adsorbent material to enhance iron removal from produced water," *UPB Sci. Bull. Ser. B Chem. Mater. Sci.*, vol. 82, no. 1, p. 237–246, 2020. [Online]. Available: https://api.semanticscholar.org/CorpusID:222089565

[18] Z. Mekhelf, A. Subhi, and R. Hamied, "Removal of iron from produced water using silica adsorbent material," *Eng. Technol. J.*, vol. 38, no. 08, pp. 1154–1159, 2020. [Online]. Available: https://doi.org/10.30684/etj.v38i8a.1125

[19] C. Vogt and B. M. Weckhuysen, "The concept of active site in heterogeneous catalysis," *Nat. Rev. Chem.*, vol. 6, no. 2, p. 89–111, 2022. [Online]. Available: https://doi.org/10.1038/s41570-021-00340-y

[20] A. Azizi, M. Forghani, L. A. Kafshgari, and A. Hassanzadeh, "Adsorptive removal behavior of pb(ii) and cr(vi) pollutants from an aqueous environment onto polyaniline-modified mil100(fe)," *Minerals*, vol. 13, no. 3, p. 299, 2023. [Online]. Available: https://doi.org/10.3390/min13030299

[21] M. A. Karim, S. Nasir, S. A. Rachman, and N.Novia, "Adsorption kinetic of mn(ii) ions in synthetic acid mine water using calcium carbide residue as an adsorbents," *J. Comput. Theor. Nanosci*, vol. 16, no. 7, p. 2892–2899, 2019. [Online]. Available: https://doi.org/10.1166/jctn.2019.8192

[22] J. N. Akoji, "Adsorption performance of packed bed column for the removal of lead (ii) using velvet tamarind (dialium indum) shells," *Asian J. Appl. Chem. Res.*, vol. 3, no. 2, p. 1–14, 2019. [Online]. Available: https://doi.org/10.9734/ajacr/2019/v3i230089

[23] Y. He, P. Wu, W. Xiao, G. Li, J. Yi, Y. He, C. Chen, P. Ding, and Y. Duan, "Efficient removal of pb(ii) from aqueous solution by a novel ion imprinted magnetic biosorbent: Adsorption kinetics and mechanisms," *PLOS ONE*, vol. 14, no. 3, pp. 1–17, 03 2019. [Online]. Available: https://doi.org/10.1371/journal.pone.0213377

[24] M. Vigdorowitsch, A. Pchelintsev, L. Tsygankova, and E. Tanygina, "Freundlich isotherm: An adsorption model complete framework," *Appl. Sci. (Switzerland)*, vol. 11, no. 17, p. 8078, 2021. [Online]. Available: https://doi.org/10.3390/app11178078

[25] J.-P. Simonin, "On the comparison of pseudo-first order and pseudo-second order rate laws in the modeling of adsorption kinetics," *Chemical Engineering Journal*, vol. 300, pp. 254–263, 2016. [Online]. Available: https://doi.org/10.1016/j.cej.2016.04.079

[26] H. N. Tran, "Applying linear forms of pseudo-second-order kinetic model for feasibly identifying errors in the initial periods of time-dependent adsorption datasets," *Water (Switzerland)*, vol. 15, no. 6, p. 1231, 2023. [Online]. Available: https://doi.org/10.3390/w15061231

[27] U. A. Edet and A. O. Ifelebuegu, "Kinetics, isotherms, and thermodynamic modeling of the adsorption of phosphates from model wastewater using recycled brick waste," *Processes*, vol. 8, no. 6, p. (665)1–15, 2020. [Online]. Available: https://doi.org/10.3390/PR8060665

[28] J. C. Bullen, S. Saleesongsom, K. Gallagher, and D. J. Weiss, "A revised pseudo-second-order kinetic model for adsorption, sensitive to changes in adsorbate and adsorbent concentrations," *Langmuir*, vol. 37, no. 10, p. 3189–3201, 2021. [Online]. Available: https://doi.org/10.1021/acs.langmuir.1c00142

[29] A. Acharya, G. Jeppu, C. R. Girish, and B. Prabhu, "Development of a multicomponent adsorption isotherm equation and its validation by modeling," *Langmuir*, vol. 39, no. 49, p. 17862–17878, 2023. [Online]. Available: https://doi.org/10.1021/acs.langmuir.3c02496

[30] E. Annan, B. Agyei-Tuffour, Y. D. Bensah, D. S. Konadu, A. Yaya, B. Onwona-Agyeman, and E. Nyankson, "Application of clay ceramics and nanotechnology in water treatment: A review," *Cogent Engineering*, vol. 5, no. 1, p. 1476017, 2018. [Online]. Available: https://doi.org/10.1080/23311916.2018.1476017

[31] A. T. P. Atheba, N. B. Allou, and P. Drogui, "Adsorption kinetics and thermodynamics study of butylparaben on activated carbon coconut based," *J. Encapsulation Adsorpt. Sci.*, vol. 8, no. 2, p. 39–57, 2018. [Online]. Available: https://doi.org/10.4236/jeas.2016.82003

[32] A. A. Al-Badaani, A. F. Hifney, M. S. Adam, and M. Gomaa, "Low-cost biosorption of fe(ii) and fe(iii) from single and binary solutions using ulva lactuca-derived cellulose nanocrystals-graphene oxide composite film," *Sci. Rep.*, vol. 13, no. 1, p. 6422, 2023. [Online]. Available: https://doi.org/10.1038/s41598-023-33386-7

[33] O. B. Apea, B. E. Akorley, E. O. Oyelude, and B. Ampadu, "Evaluation of the adsorption behavior and divalent metal ions removal efficiency of ceramic point-of-use water filter materials," *Environ. Syst. Res.*, vol. 12, no. 37, 2023. [Online]. Available: https://doi.org/10.1186/s40068-023-00322-7

[34] T. Gameiro, C. Costa, J. Labrincha, and R. M. Novais, "Reusing spent fluid catalytic cracking catalyst as an adsorbent in wastewater treatment applications," *Mater. Today Sustain*, vol. 24, p. 100555, 2023. [Online]. Available: https://doi.org/10.1016/j.mtsust.2023.100555

[35] A. M. Elewa, A. A. Amer, M. F. Attallah, H. A. Gad, Z. A. M. Al-Ahmed, and I. A. Ahmed, "Chemically activated carbon based on biomass for adsorption of fe(iii) and mn(ii) ions from aqueous solution," *Materials (Basel)*, vol. 16, no. 3, pp. 373–381, 2023. [Online]. Available: https://doi.org/10.3390/ma16031251

[36] S. K. Al Dawery, M. K. Al-Sawai, G. M. S. Al Muzami, S. H. K. Annamareddy, M. S. Al Dawari, R. H. Harharah, H. N. Harharah, and A. Amari, "Treatment of produced water using prepared activated carbon-based sewage sludge," *Separations*, vol. 10, no. 10, 2023. [Online]. Available: https://www.mdpi.com/2297-8739/10/10/519

[37] E. Kuldeyev, M. Seitzhanova, S. Tanirbergenova, K. Tazhu, E. Doszhanov, Z. Mansurov, S. Azat, R. Nurlybaev, and R. Berndtsson, "Modifying natural zeolites to improve heavy metal adsorption," *Water*, vol. 15, no. 12, 2023. [Online]. Available: https://www.mdpi.com/2073-4441/15/12/2215

[38] T. Motsi, N. A. Rowson, and M. J. H. Simmons, "Adsorption of heavy metals from acid mine drainage by natural zeolite," *Int. J.*

Miner. Process., vol. 92, no. 1–2, p. 42–48, 2009. [Online]. Available: https://doi.org/10.1016/j.minpro.2009.02.005

[39] H. Fu, Y. Li, Z. Yu, J. Shen, J. Li, M. Zhang, T. Ding, L. Xu, and S. S. Lee, "Ammonium removal using a calcined natural zeolite modified with sodium nitrate," *Journal of Hazardous Materials*, vol. 393, p. 122481, 2020. [Online]. Available: https://doi.org/10.1016/j.jhazmat.2020.122481

How to cite this article:
Netty Herawati, Subriyer Nasir, Kiagus A. Roni, and Muhammad A. Karim (2025). 'Efficient iron removal from petroleum refinery wastewater using RCC-natural clay ceramic adsorbents: An isotherm and kinetic study', Al-Qadisiyah Journal for Engineering Sciences, 18(4), pp. 368-377. https://doi.org/10.30772/qjes.2025.161210.1588